Scientific Reports

https://doi.org/10.1038/s41598-026-44632-z

Article in Press

Edelfosine induces cell cycle arrest and apoptosis in vascular smooth muscle cells to suppress neointimal hyperplasia

Received: 13 September 2025

Accepted: 12 March 2026

Published online: 25 March 2026

Cite this article as: Sun J., Gui Y., Liu Y. *et al.* Edelfosine induces cell cycle arrest and apoptosis in vascular smooth muscle cells to suppress neointimal hyperplasia. *Sci Rep* (2026). https://doi.org/10.1038/s41598-026-44632-z

Jiaxing Sun, Yu Gui, Yuxin Liu, Yanan Guo, Rosana González Granado, Liam Guetg, Warren Peng, Shenghua Zhou & Xi-Long Zheng

Edelfosine Induces Cell Cycle Arrest and Apoptosis in Vascular Smooth Muscle Cells to Suppress Neointimal Hyperplasia

Jiaxing Sun[a,b,c], Yu Gui[a], Yuxin Liu[a], Yanan Guo[a], Rosana González Granado[a], Liam Guetg[a], Warren Peng[a], Shenghua Zhou[c], Xi-Long Zheng[a*]*

Authors:

[a] Departments of Biochemistry & Molecular Biology and Physiology & Pharmacology, Cumming School of Medicine, University of Calgary, AB, Canada.

[b] Department of Cardiovascular Medicine, Center for Circadian Metabolism and Cardiovascular Disease, Southwest Hospital, Army Medical University, Chongqing, China.

[c] Department of Cardiology, the Second Xiangya Hospital of Central South University, Changsha, China.

***Corresponding Authors:**

Shenghua Zhou, MD, PhD, 139 Middle Renmin Rd, Changsha, 410011, Hunan, China, Email zhoushenghua@csu.edu.cn

Xi-Long Zheng, MD, Ph.D., GAA12-HRIC 3280 Hospital Dr NW, Calgary, AB, Canada T2N 4Z6, Email xlzheng@ucalgary.ca|/Tel: +1 (403) 220-8715

Abstract

Background: Neointimal hyperplasia, driven by abnormal proliferation and survival of vascular smooth muscle cells (VSMCs), underlies atherosclerotic stenosis and restenosis after angioplasty or stenting. Edelfosine (ET-18-OCH_3) is an alkylphospholipid with pro-apoptotic activity. We tested whether edelfosine limits pathological VSMC growth and neointimal lesion formation by enforcing cell-cycle arrest and apoptosis.

Methods: Primary VSMCs from mouse and rat aortas were exposed to edelfosine (0-15 µM). Viability (MTT) and DNA synthesis (BrdU) were quantified. DNA content and binucleation were assessed by laser scanning cytometry and immunofluorescence. Apoptosis was measured by TUNEL and by cleavage of caspase-9, -7, and -3, with the pan-caspase inhibitor Z-VAD-FMK to test caspase dependence. Apoptosis in live cells was also analyzed using Annexin V and propidium iodide staining. Intracellular Ca^{2+} was imaged and measured in fluorescent Ca^{2+} indicator-loaded cells. In vivo, carotid artery ligation in mice induced neointimal hyperplasia; edelfosine or vehicle was delivered locally, and lesion size was measured morphometrically. Vascular apoptosis was further evaluated by TUNEL.

Results: Edelfosine reduced VSMC viability and proliferation in a dose- and time-dependent manner; at 5–10 µM it suppressed BrdU incorporation by >90% and triggered extensive cell death. Cells accumulated with 4N DNA content and showed increased binucleation, consistent with G_2/M arrest and failed cytokinesis. Approximately 40% of edelfosine-treated VSMCs were TUNEL-positive versus ~5% with vehicle ($p < 0.001$), coincident with activation of caspase-9, -7, and -3; Z-VAD-FMK prevented caspase-3 cleavage and reduced TUNEL positivity. Mechanistically, edelfosine induced endoplasmic reticulum (ER) stress (increased phospho-eIF2α), upregulated Bax, and evoked a rapid rise in intracellular Ca^{2+} in the presence of extracellular Ca^{2+}. Edelfosine-induced Ca^{2+} elevation was reduced by extracellular Ca^{2+} chelation with EGTA, blockade of VGCCs with nifedipine, and perturbation of IP_3 receptor-linked Ca^{2+} pathways with 2-

APB. In vivo, edelfosine significantly reduced neointimal lesion size after carotid ligation, lowering the intima-to-lumen ratio ($p < 0.05$) and increasing TUNEL positivity within the vessel wall.

Conclusions: Edelfosine enforces G_2/M cell-cycle arrest and caspase-dependent apoptosis in VSMCs, linked to ER stress and Ca^{2+} influx, thereby limiting neointimal hyperplasia after blood flow cessation. Local edelfosine delivery may offer a dual anti-proliferative and pro-apoptotic strategy to prevent restenosis.

Keywords: edelfosine; neointimal hyperplasia; vascular smooth muscle cell; restenosis; apoptosis; cell-cycle arrest; endoplasmic reticulum stress; carotid artery ligation.

Introduction

Neointimal hyperplasia is a pathological vascular remodeling process characterized by excessive VSMC proliferation and migration into the intimal layer of the vessel wall. This process underlies atherosclerotic stenosis and restenosis after angioplasty or stenting, as the accumulation of VSMCs and extracellular matrix in the intima leads to luminal narrowing and recurrent vessel blockage. [1,2] Current clinical approaches to prevent VSMC proliferation include drug-eluting stents (DES) that locally release anti-proliferative agents such as sirolimus or paclitaxel. Sirolimus (rapamycin) halts VSMC cell cycle progression in G_1 phase by inhibiting the mTOR pathway, [3] whereas paclitaxel stabilizes microtubules and causes cell cycle arrest (at G_0/G_1 and G_2/M phases), [4,5] thereby effectively inhibiting VSMC proliferation and neointimal growth. These therapies have significantly reduced restenosis rates by limiting VSMC expansion. [1,6] However, there remains a need for alternative or complementary agents that can more completely prevent neointimal formation, especially in complex lesions.

Edelfosine (ET-18-OCH_3) is a synthetic alkyl-lysophospholipid analog originally developed as an antitumor compound. It is the prototypical member of an ether lipid class known for selective pro-apoptotic activity in malignant cells,[7-9] notably inducing apoptosis in cancer cells while sparing most normal cells.[7,10] Unlike DNA-targeting chemotherapeutics, edelfosine does not directly interfere with DNA replication; rather, it integrates into cell membranes and modulates key signaling pathways.[7] In hematologic cancer cells (e.g., leukemic T-cells), edelfosine can activate extrinsic apoptotic pathways by clustering death receptors (such as Fas/CD95) in membrane lipid rafts, leading to caspase-8 activation.[10,11] In solid tumor cells, edelfosine preferentially accumulates in the endoplasmic reticulum (ER) and triggers an ER stress response,[12,13] including inhibition of phosphatidylcholine synthesis, phosphorylation of eukaryotic initiation

factor 2α (eIF2α), upregulation of the pro-apoptotic transcription factor CHOP (GADD153), and release of Ca^{2+} from ER stores.[14] These events culminate in mitochondrial dysfunction (loss of membrane potential, cytochrome c release) and activation of the intrinsic apoptosis pathway. [11,14]

VSMCs in pathological settings can exhibit tumor cell-like phenotypic changes.[15] The capacity of edelfosine to induce an apoptotic program in actively proliferating cells rather than quiescent cells,[7,10] suggests it might be effective against hyper-proliferative vascular conditions such as neointimal hyperplasia, which is characterized by VSMC phenotypic switching and proliferation.

The carotid artery ligation model induces VSMC-driven neointimal hyperplasia without direct endothelial denudation and is widely employed to evaluate interventions targeting VSMC proliferation and medial remodeling.[2] Our previous work and that of others have shown that this model reliably produces VSMC-dominated intimal lesions, making it well-suited to assess the impact of candidate anti-neointimal therapies on VSMC survival and remodeling. [1,16] Unlike balloon or wire injury models, which involve direct mechanical endothelial denudation, the complete carotid ligation model produces neointimal hyperplasia primarily in response to blood flow cessation and altered wall shear, with lesions largely composed of VSMCs.

In this study, we investigated the effects of edelfosine on VSMC proliferation, cell-cycle progression, and apoptosis *in vitro*, as well as its efficacy in reducing neointimal lesion formation *in vivo*. We hypothesized that edelfosine, by inducing cell-cycle arrest and apoptosis in proliferating VSMCs, would attenuate neointima formation following vascular injury. Our findings demonstrate that edelfosine potently compromises VSMC viability and DNA synthesis, causes G_2/M phase arrest with associated cytokinesis

failure, and triggers caspase-mediated apoptosis through mechanisms involving ER stress and Ca^{2+} influx. Moreover, local edelfosine delivery in a mouse carotid artery ligation model significantly reduces neointimal thickening and is associated with increased VSMC apoptosis in the vessel wall. These results highlight the therapeutic potential of edelfosine as an anti-restenosis agent and provide mechanistic insight into its actions in VSMCs.

Results

Edelfosine Inhibits VSMC Viability and Proliferation

Treatment of cultured VSMCs with edelfosine caused a marked, time- and dose-dependent reduction in cell viability. By 8 h of treatment, edelfosine at concentrations ≥ 5 µM significantly decreased the number of viable VSMCs compared to untreated controls (MTT assay). At low edelfosine concentrations (1-2 µM), MTT readings showed a modest increase above control, which may reflect a hormetic response or mild stimulation of metabolic activity at sub-toxic doses. Our mechanistic analyses therefore focused on higher concentrations (5-10 µM) that robustly suppress proliferation and induce apoptosis. This cytotoxic effect was more pronounced in the absence of serum than in its presence. For example, 10 µM edelfosine reduced viable cell numbers to ~50% of control at 8 h in growth medium with 10% FBS, whereas in serum-free conditions viability was reduced to ~20% (Figure 1A). By 24 h of treatment, edelfosine induced near-complete cell death at 10-15 µM in serum-deprived conditions but left 10-20% viability in the presence of serum (Figure 1B). Because FBS appeared to attenuate edelfosine's actions, subsequent *in vitro* experiments were conducted under serum-free conditions. The raw MTT assay data (individual replicate absorbance values) are provided in the Supplementary Materials for transparency.

Edelfosine's impact on DNA synthesis paralleled its effects on viability. BrdU incorporation assays showed that VSMCs exposed to 5 µM edelfosine for 24 h had significantly lower DNA synthesis rates compared with control cells (Figure 1C-F), indicating that edelfosine prevented VSMCs from entering S phase or synthesizing DNA during the labeling period and thereby effectively inhibited proliferation. This profound suppression of BrdU-positive rate was observed in both rat (Figure 1D) and mouse (Figure 1F, ~2% vs ~15% BrdU-positive cells) primary VSMCs. Together, these

results demonstrate that edelfosine rapidly compromises VSMC viability and proliferative capacity.

Edelfosine Induces G_2/M Cell-Cycle Arrest and Cytokinesis Failure

To determine how edelfosine affects cell-cycle progression, we analyzed VSMC DNA content over time following treatment by conducting a BrdU pulse-chase assay, which enabled us to track the fate of BrdU-labeled cycling cells (Figure 2A). At 0 h, BrdU incorporation rates were comparable in both groups. In control cells, BrdU-labeled nuclei progressed to G_2/M phase and then returned to G_0/G_1 phase. In contrast, in the presence of 5 μM edelfosine, BrdU-positive cells accumulated with 4N DNA content and failed to return efficiently to G_0/G_1, indicating a block at the G_2/M phase.

Our quantitative analyses showed that by 5-10 h of chase, edelfosine-treated cultures contained significantly more cells with ≥ 4N DNA content and fewer cells with < 4N DNA content compared with controls (Figure 2B), consistent with G_2/M arrest and/or binucleation. These cytometric data were corroborated by direct visualization of enlarged, double nuclei (Figure 2C). The proportion of binucleate cells increased to >30% in response to edelfosine treatment versus 1-2% in vehicle-treated control cells (Figure 2D).

Analysis of cell-cycle regulators provided further evidence of a G_2/M arrest. Western blotting showed that edelfosine treatment led to an initial accumulation of cyclin B (a key G_2/M regulator) during the first 60 min, followed by a decline at 24 h as binucleate cells formed (Figure 2E&F). The early rise in cyclin B is consistent with cells attempting to enter mitosis but then arresting in M phase. In contrast, cyclins D and E (which regulate G_1/S progression) were moderately reduced at later time points (Figure 2E, G&H).

To examine mitotic effects in more detail, we visualized γ-tubulin (red), microtubules (α-tubulin, green), and nuclei (DAPI, blue) by immunofluorescence in control and edelfosine-treated VSMCs. Edelfosine did not visibly disrupt prometaphase, metaphase, anaphase, or telophase spindle structures, but it caused cytokinesis failure, resulting in interphase cells exhibiting a binucleate state (Figure 3).

Edelfosine Activates Apoptosis in VSMCs

We next examined whether the growth arrest and loss of viability caused by edelfosine were accompanied by apoptotic cell death. TUNEL assays showed that 24 h of treatment with 5 μM edelfosine markedly increased the proportion of TUNEL-positive cells. Representative fluorescence images and laser scanning cytometry (LSC) scattergrams showed virtually no TUNEL-positive nuclei in control cells (Figure 4A&B), whereas ~40-45% of edelfosine-treated cells were TUNEL-positive (Figure 4B&C), consistent with extensive DNA fragmentation characteristic of late-stage apoptosis.

Consistent with these findings, we detected robust activation of caspases, the executioners of apoptosis (Figure 4D-G). Immunoblot analysis demonstrated that edelfosine triggered time-dependent cleavage of caspase-9 (initiator caspase of the intrinsic pathway), caspase-7, and caspase-3 (effector caspases). Cleaved caspase-9 (p39 fragment) became evident by 6-12 h of treatment and increased further by 24 h. Similarly, cleaved caspase-7 (p17 fragment) and cleaved caspase-3 (p19 fragment) were detected in edelfosine-treated VSMCs, with levels peaking at 12-24 h. Densitometry confirmed significant increases in the cleaved/total ratios for caspase-9, -7, and -3 compared to controls (Figure 4E-G).

Phosphorylation of eIF2α (Ser51) increased more than threefold after 3 h of edelfosine exposure (Figure 4H&I). Phospho-eIF2α is a hallmark of the unfolded protein response during ER stress,[14,17] indicating that edelfosine

disrupts protein homeostasis in the ER. Bax protein levels exhibited a transient increase to peak at 0.25 h and keep elevated at 0.5-6 h (Figure 4H&J), consistent with engagement of pro-apoptotic Bcl-2 family signaling.

To confirm that apoptosis was caspase-dependent, we performed inhibitor studies. Pre-treatment of VSMCs with Z-VAD-FMK (20 μM; a pan-caspase inhibitor) effectively blocked edelfosine-induced caspase-3 cleavage (Figure 4K&L). Correspondingly, Z-VAD-FMK significantly reduced the percentage of TUNEL-positive cells from ~20% to ~5% in the presence of edelfosine (Figure 4M; $p < 0.01$ vs edelfosine alone). Thus, inhibiting caspases rescued a substantial fraction of cells from death, indicating that caspase activation is required for the execution of apoptosis in this model. Collectively, these data demonstrate that edelfosine induces caspase-dependent apoptosis in VSMCs, associated with ER stress.

Edelfosine Perturbs Intracellular Calcium Homeostasis

Given that edelfosine can promote Ca^{2+} mobilization from the endoplasmic reticulum (ER) in other cell types, [14] we examined whether intracellular Ca^{2+} signaling changes accompany its actions in VSMCs. VSMCs were loaded with the Fluo-4 Direct™ Ca^{2+} indicator and imaged by confocal microscopy at 1-min intervals for up to 2 h following addition of edelfosine (5 μM). Representative images show that Fluo-4 fluorescence was lower before, but markedly increased after edelfosine exposure for 60 minutes (Fig. 5A). Noted that there were some cells with lower Fluo-4 intensity in the background (Fig. 5A, right); this may suggest different response times between the cells. As shown in the supplementary video, individual cells exhibited variable response latency. Time-lapse imaging indicated that most cells increased fluorescence within 2 h after edelfosine exposure, indicating an elevation of cytosolic Ca^{2+}.

To probe the source of this Ca^{2+} signal, VSMCs were treated for 30 min with vehicle (DMSO) or edelfosine (5 μM) in the absence or presence of nifedipine (1 μM), 2-APB (10 μM), or EGTA (1 mM). Nifedipine was used to inhibit L-type voltage-gated Ca^{2+} channels (VGCCs), EGTA to chelate extracellular Ca^{2+}, and 2-APB as a pharmacologic probe that can interfere with IP_3 receptor-dependent ER Ca^{2+} release pathways. Edelfosine significantly increased Fluo-4 fluorescence compared to the vehicle (Fig. 5B, C). This increase was significantly attenuated by nifedipine, 2-APB, or EGTA (Fig. 5B, C), supporting a major contribution of extracellular Ca^{2+} entry and inhibitor-sensitive Ca^{2+} signaling to the edelfosine-evoked Ca^{2+} rise.

To test whether Ca^{2+} elevation contributes to edelfosine-induced apoptosis, we assessed apoptosis in live cells under serum-free conditions using Annexin V/propidium iodide (PI) staining. Edelfosine induced a significant increase in apoptosis at 3 h (Fig. 6A, B), which was partially reduced by EGTA, nifedipine, or 2-APB. Note that prolonged treatment (e.g., 5 h) with EGTA, nifedipine, or 2-APB alone induced significant apoptosis.

Edelfosine Attenuates Neointimal Formation In Vivo and Increases Lesional Apoptosis

Finally, we evaluated whether the anti-proliferative and pro-apoptotic effects of edelfosine on VSMCs in vitro translate into a beneficial outcome in vivo. Using the mouse carotid artery ligation model, perivascular delivery of edelfosine significantly suppressed neointimal hyperplasia compared with vehicle. In vehicle-treated mice, ligated carotid arteries developed substantial neointimal lesions over 14 days, often resulting in near-occlusion of the lumen in sections proximal to the ligation site (Figure 7A, Control). By contrast, edelfosine-treated arteries exhibited a markedly thinner neointima at comparable locations (Figure 7A, Edelfosine). Quantitative morphometry demonstrated that edelfosine significantly

reduced the intima-to-media and intima-to-lumen area ratios, while medial area was not significantly changed (Figure 7B-D). Importantly, no obvious vascular injury or thrombosis was observed in any edelfosine-treated artery during the 14-day period.

We next examined apoptosis in the artery wall to determine whether increased apoptosis accompanied the smaller neointima. TUNEL staining of carotid sections revealed very few apoptotic nuclei in vehicle-treated arteries (Figure 7E, Control). In contrast, edelfosine-treated arteries showed more TUNEL-positive nuclei within the neointima and media (Figure 7E, Edelfosine; arrows). Because in vivo TUNEL was assessed qualitatively in this study, these images provide supportive evidence of increased vessel wall apoptosis following local edelfosine delivery. Semi-quantitative analysis confirmed a significant increase in TUNEL-positive nuclei in edelfosine-treated arteries compared with vehicle controls (Figure 7F).

Discussion

This study provides evidence that edelfosine, a membrane-targeting antitumor lipid, can inhibit VSMC-driven neointimal hyperplasia by inducing cell-cycle arrest and apoptosis in VSMCs. We demonstrated that edelfosine rapidly reduces VSMC viability and DNA synthesis in vitro, accompanied by G_2/M phase cell-cycle arrest and robust activation of intrinsic apoptotic pathways. In a mouse carotid artery ligation model, local perivascular delivery of edelfosine led to a marked reduction in neointimal mass, correlated with increased apoptosis within the vessel wall. These findings extend edelfosine's known pro-apoptotic activity, previously documented mainly in oncogenic cells,[10,14] to vascular smooth muscle cells, and identify edelfosine as a potential therapeutic candidate for preventing restenosis and other proliferative vascular diseases.

Mechanistically, our data suggest that edelfosine triggers a cascade in VSMCs that closely mirrors its action in tumor cells. A key early effect of edelfosine is disruption of normal cell division. We observed that edelfosine-treated VSMCs accumulated in G_2/M and exhibited cytokinesis abnormalities, including failure of daughter cell separation and binucleation. The precise molecular target responsible for this G_2/M arrest remains to be elucidated. Notably, in solid tumor cells edelfosine accumulates in the ER, disrupts phosphatidylcholine synthesis, and activates the G_2/M checkpoint via ER stress-related pathways.[13,14] This ER-targeted stress response also triggers Ca^{2+} release from ER stores (via Bax/Bak) and activation of stress kinases and caspases, ultimately leading to mitochondrial-dependent apoptosis.[13,14] The convergence of G_2/M arrest, ER stress, Ca^{2+} dysregulation, and apoptosis that we observed in edelfosine-treated VSMCs is therefore highly consistent with its established pro-apoptotic signaling mechanism.

Unlike sirolimus or paclitaxel, which inhibit the mTOR pathway or directly bind tubulin and prevent microtubule depolymerization, edelfosine is not a classical spindle poison. Instead, by integrating into cellular membranes, edelfosine likely perturbs membrane microdomains and associated signaling pathways. [5,7,18] We found that edelfosine-treated cells showed an early increase in cyclin B and a marked accumulation of binucleated cells, both features compatible with cell cycle catastrophe. Cell cycle failure can result from premature or inappropriate exit from mitosis without proper chromosome segregation, often due to checkpoint failure or severe mitotic stress,[19,20] and has been linked to ER stress-induced signaling.[14] The concurrence of G_2/M arrest, ER stress, and caspase activation in our study suggests that edelfosine forces VSMCs into apoptosis.

Furthermore, a concise comparison of edelfosine with clinically commonly used DES drugs sirolimus and paclitaxel is summarized in Table 1. In our study, Edelfosine acts primarily through ER stress, enforcing G_2/M cell-cycle arrest and caspase-dependent apoptosis. To our knowledge, sirolimus inhibits mTOR and arrests VSMCs in G_1 phase, whereas paclitaxel stabilizes microtubules and causes M-phase arrest. [7,21,22] Edelfosine also appears relatively selective for proliferating VSMCs, whereas sirolimus and paclitaxel exert broader effects on immune and endothelial cells and may damage nerve cells and endothelium. [7,21-24] Furthermore, edelfosine's lipophilicity is compatible with lipid coatings for sustained local release, while sirolimus and paclitaxel require polymer carriers that can provoke foreign-body reactions or produce hydrophobic aggregates. [24,25] These distinctions support edelfosine as an ideal candidate for local vascular therapy.

Our study observed strong activation of caspase-9, -7, and -3, indicating that the intrinsic apoptotic pathway is the main driver of apoptosis in this context. This aligns with edelfosine's pro-apoptotic behavior in many solid

tumor cells, where it localizes to the ER and triggers ER stress-mediated apoptosis that converges on mitochondrial pathways.[10,14] In our VSMCs, we confirmed evidence of ER stress (increased phospho-eIF2α), which can promote apoptotic signaling via CHOP-mediated transcriptional changes-for example, upregulation of pro-apoptotic factors such as Bax and downregulation of survival factors such as Bcl-2.[19,20]

A critical aspect of edelfosine-induced ER stress in earlier studies is disruption of ER Ca^{2+} handling and Ca^{2+} mobilization.[13,14] Consistent with this concept, we observed that edelfosine rapidly elevates cytosolic Ca^{2+} in VSMCs. This Ca^{2+} rise was attenuated by chelation of extracellular Ca^{2+} with EGTA and by nifedipine, suggesting that Ca^{2+} entry from the extracellular space, potentially involving L-type VGCC activity, contributes to the signal. The response was also reduced by 2-APB, indicating that ER-associated Ca^{2+} signaling may participate as well. Taken together, these data support a model in which edelfosine perturbs Ca^{2+} homeostasis through combined extracellular Ca^{2+} entry and ER-linked mechanisms, although the specific molecular mediators remain to be defined.

Intracellular Ca^{2+} homeostasis is essential for cellular function, and Ca^{2+} overload can promote apoptosis. [26] In line with this, edelfosine enhanced apoptosis under serum-free conditions, and early apoptosis (3 h) was partially suppressed by EGTA, nifedipine, or 2-APB. These findings suggest that Ca^{2+} signaling contributes to the early phase of edelfosine-induced apoptosis, whereas later cell death likely reflects additional Ca^{2+}-independent processes downstream of sustained ER stress, cell cycle disruption, and caspase activation. Future studies using more selective inhibitors and/or genetic approaches will be required to define the Ca^{2+}-independent mechanisms underlying edelfosine-induced apoptosis.

Pro-apoptotic Bcl-2 family proteins Bax and Bak can mediate ER Ca^{2+} leak, and cells deficient in Bax/Bak show blunted ER stress-induced Ca^{2+} release and apoptosis[27]. In our experiments, Bax was upregulated by edelfosine, which could facilitate both mitochondrial outer membrane permeabilization and ER membrane pore formation to augment Ca^{2+} release. Thus, our data support a model in which edelfosine's integration into the ER membrane initiates an unfolded protein response and Ca^{2+} dysregulation, which in turn activate the mitochondrial apoptotic pathway via Bax and caspase-9. It would be informative in future studies to test whether overexpression of anti-apoptotic Bcl-2 or use of chemical chaperones that alleviate ER stress can attenuate edelfosine-induced VSMC death, as has been shown in cancer cells.[10]

From a therapeutic perspective, the ability of edelfosine to reduce neointimal formation is particularly noteworthy. Neointimal hyperplasia after vascular injury is driven largely by VSMC proliferation and migration and represents a major cause of failure in revascularization procedures. Similar to traditional anti-proliferative agents (sirolimus, paclitaxel, etc.) that halt VSMC growth, edelfosine appears to both arrest the cell cycle (preventing new proliferation) and actively trigger cell death in VSMCs that would otherwise accumulate in the vascular wall. This dual action could make it a potent inhibitor of intimal hyperplasia. The concept of therapeutically inducing VSMC apoptosis to limit neointimal thickening has been explored in other contexts; for example, a one-time treatment with epothilone D (a microtubule stabilizer similar to paclitaxel) delivered via balloon catheter increased VSMC apoptosis and reduced neointimal area in rat carotid arteries.[28] Our findings with edelfosine support this paradigm: targeting VSMC survival as well as proliferation can yield strong suppression of lesion growth.

However, the extent and timing of VSMC apoptosis are critical. Excessive loss of VSMCs in blood vessels could potentially weaken the vessel wall or, in atherosclerotic plaques, promote instability. In our short-term, controlled injury model, edelfosine-induced VSMC apoptosis was associated with a favorable outcome (smaller neointima) and no obvious adverse effects on vessel structure. Although we did not systematically quantify overall vessel diameter as a primary endpoint, reduced neointimal mass could influence remodeling responses, potentially favoring mild inward remodeling. The media appeared intact in H&E sections, and no aneurysm, rupture or thrombosis was observed during the 14-day period. Future studies should examine longer-term effects and whether the vessel heals with a stable, re-endothelialized surface.

An advantage of edelfosine as a candidate therapeutic is its relative selectivity and tolerability. In previous cancer trials, edelfosine showed limited systemic toxicity and tended to accumulate in target tissues (e.g., tumors or, potentially, the treated vessel area) due to its lipophilic nature. Edelfosine has been reported to induce a caspase-dependent apoptotic program preferentially in actively proliferating cells, while largely sparing quiescent cells. [18] Nevertheless, our present study evaluated only a short-term, local intervention (14 days). Additional work is needed to explore potential long-term effects on vascular remodeling, including the risk of adverse constrictive or expansive remodeling. We did not perform in vivo co-staining for α-SMA or CD31 on the TUNEL-stained sections, nor did we measure proliferation markers (e.g., Ki67) or ER stress markers (e.g., CHOP, BiP) in the ligated arteries. We provide semi-quantitative analysis of in vivo TUNEL staining (Fig. 7F); however, definitive attribution of TUNEL-positive nuclei to specific cell types remains a limitation without α-SMA/CD31 co-staining. On the basis of the known cellular composition of carotid ligation lesions and the localization of TUNEL-positive nuclei within the neointima and media, we infer that many apoptotic nuclei are likely

VSMCs. Nevertheless, definitive cell-type attribution and in vivo confirmation of ER stress signaling will require future studies incorporating cell-specific markers and additional histological endpoints.

Despite the clear anti-hyperplastic effects observed, our study has certain limitations. We did not directly assess VSMC migration, which is a key contributor to neointimal lesion development alongside proliferation.[29] Future studies should examine whether edelfosine modulates VSMC migratory capacity, as migration strongly influences intimal hyperplasia outcomes. Additionally, the impact of edelfosine on endothelial recovery was not evaluated; because timely re-endothelialization can mitigate neointima formation, it will be important to confirm that edelfosine does not impair endothelial regrowth. Finally, our observations were limited to a relatively short post-injury period; longer-term studies are needed to determine whether edelfosine's suppression of neointimal growth is sustained and to monitor any late-occurring vascular remodeling. Furthermore, our mechanistic experiments used primary rodent VSMCs, it will be important to determine whether human arterial VSMCs exhibit similar sensitivity to edelfosine-induced G_2/M arrest and apoptosis. Such studies will be essential before considering clinical translation.

Conclusions

Edelfosine, a pro-apoptotic ether lipid, potently inhibits VSMC proliferation and viability by inducing G_2/M cell-cycle arrest and caspase-dependent apoptosis. The apoptotic response is mediated via the intrinsic mitochondrial pathway, likely initiated by ER stress and associated with Ca^{2+} influx from extracellular sources. In a mouse carotid artery ligation model, local edelfosine treatment produced a significant reduction in neointimal hyperplasia, concomitant with increased apoptosis within the neointima/media (TUNEL-positive nuclei). These findings suggest that edelfosine can limit pathological vascular remodeling through combined anti-proliferative and pro-apoptotic actions on VSMCs. Edelfosine therefore

holds promise as a novel therapeutic approach for preventing restenosis after angioplasty or stenting and warrants further exploration in preclinical and clinical settings.

Materials and Methods

Materials

Male C57BL/6J mice were obtained from The Jackson Laboratory (Bar Harbor, ME). Primary rat vascular smooth muscle cells (VSMCs) were cultured from the aortas of Sprague-Dawley rats (Charles River, Laval, QC, Canada), and primary mouse VSMCs were cultured from the aortas of C57BL/6J mice. Z-VAD-FMK (Cat. No. 7023) was obtained from SelleckChem (Burlington, ON, Canada). Collagenase type II (CAS 9001-12-1), Dulbecco's modified Eagle medium (DMEM)/F-12 (#2323609), Ham's F-12 nutrient medium (Thermo Fisher Scientific, #11330), penicillin (10,000 U/mL; #15140122), streptomycin (10,000 µg/mL; #15140122), fetal bovine serum (FBS; #A4766801), BrdU (5-bromo-2′-deoxyuridine) mouse monoclonal antibody (#MA1-19213), and the Fluo-4 Direct™ Calcium Assay Kit (F10471), were purchased from Thermo Fisher Scientific (Mississauga, ON, Canada). MTT (thiazolyl blue tetrazolium bromide; #M5655), BrdU (nucleoside; #B5002), propidium iodide (PI; #P4170), hydroxyurea (HU; #H8627), Annexin V-FITC Apoptosis Detection Kit II (# CBA059) and sterile hydrogel (#P2443) were from MilliporeSigm (Oakville, ON, Canada).

The senescence-associated β-galactosidase (SA-β-gal) staining kit (#9860S) and primary antibodies for cyclin B1 (#12231), cyclin D1 (#2936), cyclin E1 (#4132), caspase-3 (#14220), cleaved caspase-3 (#9664), GAPDH (#5174), caspase-7 (#12827), cleaved caspase-7 (#8438), caspase-9 (#9508), cleaved caspase-9 (#52873), Bax (#2772), eIF2α (#9722), phospho-eIF2α (#9721), and goat anti-rabbit secondary antibody (#7074P2) were purchased from Cell Signaling Technology (Whitby, ON, Canada). The In Situ Cell Death Detection Kit (TUNEL) was purchased from Roche (Mississauga, ON, Canada). Enhanced chemiluminescence (ECL) solution was obtained from Bio-Rad (Mississauga, ON, Canada).

Cell Culture and Treatment

Primary rat aortic VSMCs were isolated and cultured following a previously established protocol. [30] Briefly, rat aortas were dissected and freed from adhering adipose tissue, after which the adventitial layer was carefully stripped and the intimal surface thoroughly scraped to remove non-target cells. The processed aortas were then cut into small fragments (~1 mm^3) for explant culture, and tissues were maintained undisturbed for approximately 2 h before addition of DMEM/F-12 medium supplemented with 20% FBS. Upon reaching subconfluence, cells were subcultured in DMEM/F-12 medium containing 10% FBS plus penicillin-streptomycin.

Primary mouse aortic VSMCs were cultured according to a previously described method. [31] In brief, mouse aortas were isolated, the adventitia was removed, and the vessel was cut into small pieces (1-2 mm). Tissue fragments were digested with 1.5 mg/mL type II collagenase for 4-6 h at 37°C (5% CO_2). Digestion was stopped by adding complete culture medium, and samples were centrifuged at 300 × g for 5 min. The resulting cell pellet was resuspended and cultured in DMEM/F-12 medium supplemented with 10% FBS.

Primary VSMCs between passages 3 and 8 were used for all experiments. For serum-deprivation studies, cells were switched to 0.5% FBS medium for 24 h prior to treatment. Edelfosine (≥99% purity; MedChemExpress) was dissolved in ethanol and added to cultures at 5-15 μM. Control cells received vehicle (0.1% ethanol). All in vitro assays were performed in triplicate and repeated at least three times.

Cell Viability, BrdU Incorporation, and Cell Cycle Analysis

VSMCs were seeded into 96-well plates (2 × 10^3 cells/well) and allowed to attach overnight. After treatment with edelfosine or vehicle for 24 h, 20 μL of MTT reagent (5 mg/mL in PBS) was added to each well, and plates were incubated for 4 h at 37°C. Formazan crystals were then solubilized in

DMSO (150 µL/well), and absorbance at 570 nm (reference 630 nm) was measured with a microplate reader, as previously reported[32]. Cell viability was calculated as a percentage of untreated controls. All experiments were performed at least three independent times.

To assess DNA synthesis, we used a BrdU incorporation pulse-chase assay with laser scanning cytometry (LSC) as described previously.[33] VSMCs were treated with 5 µM edelfosine or vehicle for 0, 2, 6, 8, or 12 h, then pulse-labeled with 10 µM BrdU for 60 min. Cells were fixed in ice-cold 70% ethanol, treated with RNase A (100 µg/mL), and stained with 50 µg/mL PI. Incorporated BrdU was detected using an anti-BrdU antibody followed by Alexa Fluor 488-conjugated secondary antibody. Nuclei were counterstained with PI and analyzed by LSC (≥1,000 cells/area per condition), as previously described.[33] Cell-cycle distribution (% G_0/G_1, S, G_2/M) was calculated using CompuCyte software.

Immunofluorescence Microscopy

To observe cells at distinct cell-cycle phases, VSMCs grown on glass coverslips were treated with vehicle or 5 µM edelfosine for 8 h, fixed in 4% paraformaldehyde, and permeabilized with 0.2% Triton X-100. After blocking with 5% BSA, cells were stained with antibodies against α-tubulin (1:250) or γ-tubulin (1:300). Cells were then incubated with goat anti-rabbit Alexa Fluor 488 (1:400) or goat anti-mouse Rhodamine Red (1:400) for 60 min at 37°C. Nuclei were counterstained with DAPI. Mitotic abnormalities and binucleation were examined with an Olympus FV10i confocal microscope. Binucleated cells were quantified from three independent experiments.

Western Blotting

VSMCs were lysed in radioimmunoprecipitation assay (RIPA) buffer containing protease and phosphatase inhibitors (Roche). Lysates were

centrifuged at 14,000 × g for 15 min at 4°C, and protein concentrations were determined by BCA assay. Equal amounts of protein were separated by SDS-PAGE and transferred to PVDF membranes. After blocking with 5% nonfat milk, membranes were incubated with primary antibodies against cleaved/total caspase-3 (1:1000), cleaved/total caspase-7 (1:1000), cleaved/total caspase-9 (1:1000), Bax (1:1000), phospho- eIF2α/total eIF2α (1:500), cyclin B1 (1:1000), cyclin D1 (1:1000), cyclin E1 (1:1000), and α-tubulin (1:1000). After incubation with HRP-conjugated goat anti-rabbit or goat anti-mouse secondary antibodies (1:5000), bands were visualized using ECL and imaged on a Bio-Rad ChemiDoc system. Densitometry was performed using ImageJ; protein levels were normalized to β-actin, α-tubulin, or the total form of the target protein, as appropriate.

Caspase Inhibition Assay

To assess the role of caspases, rat VSMCs were pretreated with Z-VAD-FMK (20 μM; SelleckChem) or vehicle for 1 h, then exposed to 5 μM edelfosine for 24 h. Apoptosis was evaluated by TUNEL staining, and cleaved caspase-3 was analyzed by Western blot.

Apoptosis Detection

TUNEL assay: after 24 h of treatment, VSMCs on coverslips were fixed in 4% paraformaldehyde, permeabilized with 0.1% Triton X-100, and processed using the Roche In Situ Cell Death Detection Kit (Roche). Samples were incubated with terminal deoxynucleotidyl transferase (TdT) and fluorescein-labeled dUTP for 1 h at 37°C. Nuclei were counterstained with PI or DAPI. TUNEL-positive cells were imaged by fluorescence microscopy and quantified using LSC (≥1,000 cells/condition).

To directly evaluate cellular responses to edelfosine, apoptosis was also assessed in live cells using the Annexin V-FITC Apoptosis Detection Kit II, which detects early apoptotic cells (Annexin V-positive) and late apoptotic

cells (Annexin V-positive and propidium iodide [PI]-positive). VSMCs were cultured in 24-well plates in DMEM containing 10% FBS for 24 h, then switched to phenol-red-free DMEM and treated as indicated for 3-5 h. Cells were washed with PBS and stained with Annexin V-FITC and PI according to the manufacturer's instructions; Hoechst 33342 was used to counterstain nuclei. Live-cell images were acquired using an Olympus IX70 fluorescence microscope (Tokyo, Japan) with SPOT 5.0 software (Diagnostic Instruments, MI). Apoptosis was quantified in ImageJ as the percentage of Annexin V-positive and/or PI-positive cells relative to total cells.

Intracellular Calcium Measurement and Imaging

Intracellular Ca^{2+} was measured using the Fluo-4 Direct™ Calcium Assay Kit according to the manufacturer's instructions with minor modifications. For time-lapse confocal imaging, rat VSMCs cultured on glass-bottom 35-mm dishes for 24 h were loaded with an equal volume of 2× Fluo-4 Direct™ reagent loading solution and incubated at 37°C for 60 min. Cells were then stimulated with edelfosine (5 µM), and fluorescence was recorded at 1-min intervals for up to 2 h using a confocal microscope (Olympus FV10i, Tokyo, Japan; excitation 494 nm, emission 516 nm). Time-lapse image sequences were compiled into a movie file using Microsoft Clipchamp software. For fluorescence intensity quantification and inhibitor experiments, VSMCs cultured in 24-well plates were loaded with Fluo-4 Direct™ as above, then treated as indicated for 30 min in phenol-red-free DMEM (containing 1.3 mM Ca^{2+}). Hoechst 33342 was used to counterstain nuclei. Images were acquired using an Olympus IX70 fluorescence microscope with SPOT 5.0 software, and Fluo-4 fluorescence intensity was quantified using ImageJ as the averaged cell fluorescence intensity.

Animal Model of Neointimal Formation

All procedures were approved by the Institutional Animal Care and Use Committee (IACUC) of the University of Calgary and followed NIH

guidelines. Male C57BL/6J mice (10-12 weeks old, ~25 g) were randomized into vehicle or edelfosine treatment groups (vehicle n = 5; edelfosine n = 6). Under isoflurane anesthesia, the left common carotid artery was completely ligated near the bifurcation as described previously. [16] A 100 µL hydrogel containing 50 µM edelfosine (in PBS with 0.5% ethanol) or vehicle was applied perivascularly around the exposed artery immediately after ligation. Mice received postoperative analgesia and were euthanized 14 days post-surgery for analysis.

Histology and Morphometric Analysis

Carotid arteries were perfusion-fixed in situ with 4% paraformaldehyde and embedded in paraffin. Serial cross-sections (5 µm) were collected every 200 µm along a 1.6 mm segment proximal to the ligation site. Sections were stained with hematoxylin and eosin (H&E) and imaged at 10×–20× magnification. Intimal, medial, and luminal areas were measured using ImageJ, and the intima-to-media and intima-to-lumen area ratios were calculated. Adjacent sections were stained for apoptosis using a fluorescent TUNEL kit (Millipore) and counterstained with propidium iodide (PI). For semi-quantitative analysis, TUNEL-positive nuclei defined by co-localization of TUNEL signal with PI and were expressed as a percentage of total PI-positive nuclei within the vessel wall (neointima + media). All analyses were performed by an observer blinded to the treatment groups.

Statistical Analysis

All data are expressed as mean ± SD or mean ± SEM, as indicated in the figure legends. Unless otherwise stated, in vitro experiments were repeated at least three independent times (n denotes independent experiments), and for animal studies n denotes the number of mice. GraphPad Prism (v8.3.0) and IBM SPSS Statistics (v26) were used for statistical analyses. The Shapiro–Wilk test was used to assess data normality. For two-group comparisons, an unpaired Student’s t-test was used for normally distributed

data, and the Mann–Whitney U test for non- normal data. For experiments involving multiple groups or two groups under multiple treatment conditions, one-way ANOVA with Dunnett's post hoc test or two-way ANOVA with Sidak's post hoc test was used as appropriate. Repeated-measures ANOVA coupled with Dunnett's post hoc test was used for time-course or spatial measurements across multiple points. All tests were two-tailed, and a P-value < 0.05 was considered statistically significant.

Table 1. Comparison of Edelfosine with Sirolimus and Paclitaxel (DES Drugs)

Feature	Edelfosine	Sirolimus	Paclitaxel	References
Core Mechanism of Action	ER- stress, enforcing; induction; enforces G_2/M cell-cycle arrest and caspase-dependent apoptosis in VSMCs	mTOR pathway inhibition, arresting; G_1 cell-cycle arrest in VSMCs at G1 phase	Microtubule stabilization; M-phase arrest, blocking VSMC (blocks mitosis (M phase arrest)	7,21,22
VSMC Selectivity	High (preferentially inhibits targets proliferating VSMCs)	Low (also inhibits immune cells and& endothelial cells)	Low (damages nerve cells and endothelial cells, neurons)	7,21-24
Delivery Considerati	Lipophilicity; amenable to lipid coating, achieving coatings-based coatings for local sustained release	Polymer Requires polymer carrier-dependent; prone to; potential foreign -body	Strong hydrophobicity; prone to aggregation and tissue accumulation	24,25

reaction

response

List of Abbreviations

Abbreviations: 2-APB, 2-aminoethoxydiphenyl borate; BrdU, 5-bromo-2′-deoxyuridine; DES, drug-eluting stent(s); DMSO, dimethyl sulfoxide; EGTA, ethylene glycol-bis(β-aminoethyl ether)-N,N,N′,N′-tetraacetic acid; ER, endoplasmic reticulum; FBS, fetal bovine serum; IP_3, inositol trisphosphate; MTT, thiazolyl blue tetrazolium bromide; PI, propidium iodide; SOCE, store-operated calcium entry; TUNEL, terminal deoxynucleotidyl transferase dUTP nick end labeling; VGCCs, voltage-gated calcium channels; VSMC, vascular smooth muscle cell.

(Any other abbreviations used in the text are defined at first mention.)

Declarations

Ethics approval and consent to participate

All animal experiments were approved by the Institutional Animal Care and Use Committee of the University of Calgary and were conducted in accordance with the NIH Guide for the Care and Use of Laboratory Animals. This article does not contain any studies with human participants; therefore, human consent was not required.

ARRIVE guidelines

Sample size:

Sample size calculation was not performed (no a priori power calculation was conducted).

Inclusion criteria:

Healthy, age-matched adult mice as detailed in Materials and Methods.

Exclusion criteria:

Mice with dysplastic teeth.

Randomization:

Animals were randomized when assigning to experimental groups.

Blinding:

Blinding was not performed during data acquisition and analysis.

Consent for publication: Not applicable (no human subjects or identifiable data).

Availability of data and materials

All data generated or analyzed during this study are included in this published article and its supplementary information files. Additional raw

data and materials are available from the corresponding author on reasonable request.

Competing interests

The authors declare that they have no competing interests.

Funding

This work was supported by the Canadian Institutes of Health Research (CIHR; Project Grants PJT-178010 and PJT-165941 to X-L.Z.), the Heart & Stroke Foundation of Canada (G-22-0032035 to X-L.Z.), and the Natural Sciences and Engineering Research Council of Canada (RGPIN-2020-04592 to X-L.Z.).

Authors' contributions:

Xi-Long Zheng, Jiaxing Sun and Shenghua Zhou conceived and designed the study. Jiaxing Sun, Yu Gui and Yuxin Liu carried out the in vitro experiments and data analysis. Yanan Guo and Jiaxing Sun performed the animal surgery and in vivo data collection. Rosana González Granado, Liam Guetg, and Warren Peng assisted with data interpretation and provided critical reagents. Jiaxing Sun, Xi-Long Zheng and Yu Gui drafted the manuscript with input from all authors. All authors read and approved the final manuscript.

Acknowledgements

Not applicable.

Figure Legends

Figure 1. Edelfosine inhibits VSMC viability and DNA synthesis.
(A, B) Rat aortic VSMCs were cultured in DMEM/F-12 medium with or without 10% FBS and exposed to the indicated concentrations of edelfosine (Edel) for 8 h (A) or 24 h (B). Cell viability was quantified by MTT assay and expressed as a percentage of vehicle (ethanol) control (mean ± SEM, n = 3-4 per group). (C-F) Primary VSMCs (rat in C-D, mouse in E-F) were serum-deprived for 24 h, then treated with 5 µM edelfosine or ethanol (vehicle) for the indicated times. Cells were pulse-labeled with BrdU (10 µM, 60 min) prior to fixation and analyzed by LSC. (C, E) Representative BrdU vs PI scattergrams; BrdU-positive nuclei are in the upper two quadrants (red events). (D, F) BrdU labeling index (% of nuclei that were BrdU-positive) at each time point (mean ± SEM, n = 3 independent experiments). *p < 0.05, **p < 0.01, ***p < 0.001 vs control.

Figure 2. Edelfosine arrests VSMCs in G_2/M and promotes binucleation.
VSMCs were labeled with BrdU for 1 h, then chased in ethanol or 5 µM edelfosine for 0, 2, 6, 8, 10, or 12 h before fixation. (A) BrdU/PI scattergrams (upper) and DNA content histograms (lower) at the indicated chase times, comparing control (top row) vs edelfosine-treated (bottom row) cells. In edelfosine-treated cells, note the rise in the 4N (G_2/M) population by 2 h and reduced return of labeled cells to G_0/G_1 at later time points. (B) Distribution of cells with < 4N (G_0/G_1/S) or ≥ 4N (G_2/M or binucleate) DNA content at each time (mean ± SEM, n = 3). Edelfosine significantly increased the ≥ 4N fraction at 6 h. (C) Immunofluorescence images of VSMCs 24 h after treatment: α-tubulin (green) and DAPI (blue). Arrows indicate representative binucleated cells (cells with two nuclei). Scale bar = 100 µm. (D) Quantification of binucleated cells as a percentage of total cells (mean ± SEM, n = 3 fields per condition). (E) Representative Western blots showing levels of cyclin B1, cyclin D1, and cyclin E at 0, 6, 12, and 24 h

after 5 μM edelfosine treatment. α-Tubulin serves as a loading control. (F-H) Densitometric analysis of cyclin levels over time, normalized to β-actin and expressed relative to time 0. Cyclin B1 (F) rose transiently at 1 h and decreased by 24 h. Cyclin D1 (G) and cyclin E (H) showed modest declines at 12-24 h. *$p < 0.05$, **$p < 0.01$.

Figure 3. Edelfosine disrupts cytokinesis without grossly altering mitotic spindle morphology.

Immunofluorescence analysis of the cell-cycle in control and edelfosine-treated VSMCs. Cells were co-stained for α-tubulin (green, microtubules), γ-tubulin (red, centrosomes), and DNA (DAPI, blue). Representative confocal images of VSMCs in prometaphase, metaphase, anaphase, telophase, cytokinesis, and interphase are shown. Edelfosine-treated cultures show an increased frequency of binucleated interphase cells, consistent with cytokinesis failure.

Figure 4. Edelfosine induces ER stress and caspase-dependent apoptosis in VSMCs.

(A-C) TUNEL assays of VSMCs after 24 h treatment. (A) Fluorescence micrographs of cells stained by TUNEL (green) and PI for nuclei (red). Control cells (left) show virtually no TUNEL-positive nuclei, whereas edelfosine-treated cells (right) exhibit abundant TUNEL-positive nuclei (examples indicated by arrows). Scale bar = 50 μm. (B) Representative LSC scattergrams plotting PI intensity vs TUNEL fluorescence per nucleus. In edelfosine-treated samples, a distinct population of TUNEL-positive events appears (upper quadrants, red dots). (C) Quantification of the percentage of TUNEL-positive cells (mean ± SEM, n = 5). (D-J) Time-course Western blots showing activation of apoptotic proteins in VSMCs treated with 5 μM edelfosine. (D) Immunoblots for cleaved caspase-9 (39 kDa), cleaved caspase-7 (17 kDa), and cleaved caspase-3 (19 kDa). Cleavage increased over 6-24 h. Blots for total caspases are shown as loading controls. (E-G)

Densitometric ratios of cleaved/total caspase-9, -7, and -3, respectively (mean ± SEM, n = 3). (H) Blots for phospho-eIF2α (p-eIF2α), total eIF2α, and Bax at the indicated times; α-tubulin was the loading control. (I, J) Quantification of p-eIF2α relative to total eIF2α (I) and Bax relative to α-tubulin (J). (K-M) Effect of caspase inhibition on edelfosine-induced apoptosis. VSMCs were pretreated ± 20 μM Z-VAD-FMK (pan-caspase inhibitor) for 1 h, then 5 μM edelfosine was added for 10 h. (K) Western blot for cleaved caspase-3. Edelfosine alone (+vehicle) shows strong caspase-3 cleavage, which is abolished by Z-VAD-FMK. (L) Densitometry of cleaved caspase-3 bands (normalized to tubulin, mean ± SEM, n = 3). (M) TUNEL-positive fraction of cells under each condition (mean ± SEM, n = 3). Z-VAD-FMK significantly reduced edelfosine-induced apoptosis. *$p < 0.05$, **$p < 0.01$, ***$p < 0.001$ vs vehicle.

Figure 5. Edelfosine elevates cytosolic Ca^{2+} and is sensitive to Ca^{2+} pathway inhibition. Intracellular Ca^{2+} levels were monitored in VSMCs using Fluo-4 as the Ca^{2+} indicator. (A) Representative confocal images before (left) and after (right) edelfosine stimulation. Cells were loaded with Fluo-4 for 60 min and imaged at 1-min intervals for up to 2 h. Note that some cells show lower fluorescence at a given time point due to variable response latency (see Supplementary Video). (B) Representative images of VSMCs treated with DMSO vehicle, edelfosine, or edelfosine in the presence of EGTA, nifedipine, and 2-APB, respectively, in phenol-red-free DMEM for 30 min. (C) Quantification of mean fluorescence intensity from three independent experiments. *$p < 0.001$ vs vehicle; **$p < 0.01$ vs edelfosine.

Figure 6. Edelfosine-induced increase in intracellular Ca^{2+} is involved in short-term apoptosis.
(A) Representative images of cells stained with Annexin V, PI, and Hoechst after 3 h treatment with DMSO, edelfosine, or edelfosine in the presence of EGTA, nifedipine, and 2-APB, respectively, in phenol-red-free DMEM. (B)

Quantification of the percentages of early apoptotic cells (Annexin V-positive) and late apoptotic cells (PI-positive) relative to total cells (Hoechst-positive) after 3 h treatment, as indicated. *p < 0.01 vs vehicle; **p < 0.01 vs edelfosine; n = 3.

Figure 7. Perivascular edelfosine limits neointimal hyperplasia after carotid ligation. Male C57BL/6J mice underwent complete ligation of the left common carotid artery (LCA) to induce neointimal formation. A hydrogel loaded with edelfosine (100 µL, 50 µM) or vehicle was applied perivascularly around the ligated artery (vehicle n = 5; edelfosine n = 6). Analysis was performed 14 days post-ligation. (A) Representative cross-sections stained with hematoxylin and eosin (H&E) ~0.4 mm proximal to the ligation site. Vehicle-treated arteries develop a thick neointima (NI) that markedly narrows the lumen, whereas edelfosine-treated arteries show substantially less neointimal thickening; the media (M) appears intact. Scale bar, 200 µm. (B–D) Medial area, intima-to-media area ratio, and intima-to-lumen area ratio quantified at distances 400-1600 µm from the ligation site. Data are mean ± SEM (vehicle n = 5; edelfosine n = 6). *p < 0.05 vs vehicle. (E) TUNEL staining (green) with propidium iodide (PI) nuclear counterstain (red). Representative images from the cohort quantified in (F) show few TUNEL-positive nuclei in vehicle-treated arteries and increased TUNEL-positive nuclei within the neointima and media after edelfosine treatment (arrows). Scale bar, 200 µm. (F) Semi-quantitative analysis of TUNEL staining, expressed as TUNEL-positive nuclei (co-localized with PI) as a percentage of total nuclei in the vessel wall. Data are mean ± SEM (vehicle n = 4; edelfosine n = 3). *p < 0.05 vs vehicle.

References

1 Marx, S. O., Totary-Jain, H. & Marks, A. R. Vascular smooth muscle cell proliferation in restenosis. *Circ Cardiovasc Interv* **4**, 104-111, doi:10.1161/circinterventions.110.957332 (2011).

2 Déglise, S., Bechelli, C. & Allagnat, F. Vascular smooth muscle cells in intimal hyperplasia, an update. *Front Physiol* **13**, 1081881, doi:10.3389/fphys.2022.1081881 (2022).

3 Sun, J. *et al.* Role for p27(Kip1) in Vascular Smooth Muscle Cell Migration. *Circulation* **103**, 2967-2972, doi:10.1161/01.cir.103.24.2967 (2001).

4 Herdeg, C. *et al.* Local paclitaxel delivery for the prevention of restenosis: biological effects and efficacy in vivo. *J Am Coll Cardiol* **35**, 1969-1976, doi:10.1016/s0735-1097(00)00614-8 (2000).

5 Axel, D. I. *et al.* Paclitaxel inhibits arterial smooth muscle cell proliferation and migration in vitro and in vivo using local drug delivery. *Circulation* **96**, 636-645, doi:10.1161/01.cir.96.2.636 (1997).

6 Morice, M. C. *et al.* A randomized comparison of a sirolimus-eluting stent with a standard stent for coronary revascularization. *N Engl J Med* **346**, 1773-1780, doi:10.1056/NEJMoa012843 (2002).

7 Mollinedo, F., Gajate, C., Martín-Santamaría, S. & Gago, F. ET-18-OCH3 (edelfosine): a selective antitumour lipid targeting apoptosis through intracellular activation of Fas/CD95 death receptor. *Current medicinal chemistry* **11**, 3163-3184, doi:10.2174/0929867043363703 (2004).

8 Mollinedo, F. Editorial: Antitumor alkylphospholipid analogs: a promising and growing family of synthetic cell membrane-targeting molecules for cancer treatment). *Anti-cancer agents in medicinal chemistry* **14**, 495-498, doi:10.2174/1871520614999140313160011 (2014).

9 Jaffrès, P. A. *et al.* Alkyl ether lipids, ion channels and lipid raft reorganization in cancer therapy. *Pharmacology & therapeutics* **165**, 114-131, doi:10.1016/j.pharmthera.2016.06.003 (2016).

10 Gajate, C. & Mollinedo, F. Edelfosine and perifosine induce selective apoptosis in multiple myeloma by recruitment of death receptors and downstream signaling molecules into lipid rafts. *Blood* **109**, 711-719, doi:10.1182/blood-2006-04-016824 (2007).

11 Mollinedo, F. & Gajate, C. Mitochondrial Targeting Involving Cholesterol-Rich Lipid Rafts in the Mechanism of Action of the Antitumor Ether Lipid and Alkylphospholipid Analog Edelfosine. *Pharmaceutics* **13**, doi:10.3390/pharmaceutics13050763 (2021).

12 Bonilla, X., Dakir el, H., Mollinedo, F. & Gajate, C. Endoplasmic reticulum targeting in Ewing's sarcoma by the alkylphospholipid analog edelfosine. *Oncotarget* **6**, 14596-14613, doi:10.18632/oncotarget.4053 (2015).

13 Mollinedo, F. & Gajate, C. Direct Endoplasmic Reticulum Targeting by the Selective Alkylphospholipid Analog and Antitumor Ether Lipid Edelfosine as a Therapeutic Approach in Pancreatic Cancer. *Cancers* **13**, doi:10.3390/cancers13164173 (2021).

14 Nieto-Miguel, T. *et al.* Endoplasmic reticulum stress in the proapoptotic action of edelfosine in solid tumor cells. *Cancer Res* **67**, 10368-10378, doi:10.1158/0008-5472.Can-07-0278 (2007).

15 Pan, H. *et al.* Atherosclerosis Is a Smooth Muscle Cell-Driven Tumor-Like Disease. *Circulation* **149**, 1885-1898, doi:10.1161/circulationaha.123.067587 (2024).

16 Sun, J. *et al.* Polo-like kinase 4 inhibitor CFI-400945 inhibits carotid arterial neointima formation but increases atherosclerosis. *Cell death discovery* **9**, 49, doi:10.1038/s41420-023-01305-4 (2023).

17 Guo, L. *et al.* Phosphorylated eIF2α predicts disease-free survival in triple-negative breast cancer patients. *Scientific reports* **7**, 44674, doi:10.1038/srep44674 (2017).

18 Gajate, C. & Mollinedo, F. Biological activities, mechanisms of action and biomedical prospect of the antitumor ether phospholipid ET-18-OCH(3) (edelfosine), a proapoptotic agent in tumor cells. *Curr Drug Metab* **3**, 491-525, doi:10.2174/1389200023337225 (2002).

19 Hu, H., Tian, M., Ding, C. & Yu, S. The C/EBP Homologous Protein (CHOP) Transcription Factor Functions in Endoplasmic Reticulum Stress-Induced Apoptosis and Microbial Infection. *Front Immunol* **9**, 3083, doi:10.3389/fimmu.2018.03083 (2018).

20 McCullough, K. D., Martindale, J. L., Klotz, L. O., Aw, T. Y. & Holbrook, N. J. Gadd153 sensitizes cells to endoplasmic reticulum stress by down-regulating Bcl2 and perturbing the cellular redox state. *Mol Cell Biol* **21**, 1249-1259, doi:10.1128/mcb.21.4.1249-1259.2001 (2001).

21 McKeage, K., Murdoch, D. & Goa, K. L. The sirolimus-eluting stent: a review of its use in the treatment of coronary artery disease. *American journal of cardiovascular drugs : drugs, devices, and other interventions* **3**, 211-230, doi:10.2165/00129784-200303030-00007 (2003).

22 Stone, G. W. *et al.* Paclitaxel-eluting stents versus bare-metal stents in acute myocardial infarction. *N Engl J Med* **360**, 1946-1959, doi:10.1056/NEJMoa0810116 (2009).

23 Gajate, C. & Mollinedo, F. Lipid raft-mediated Fas/CD95 apoptotic signaling in leukemic cells and normal leukocytes and therapeutic implications. *Journal of leukocyte biology* **98**, 739-759, doi:10.1189/jlb.2MR0215-055R (2015).

24 Stone, G. W. *et al.* A polymer-based, paclitaxel-eluting stent in patients with coronary artery disease. *N Engl J Med* **350**, 221-231, doi:10.1056/NEJMoa032441 (2004).

25 Katz, G., Harchandani, B. & Shah, B. Drug-eluting stents: the past, present, and future. *Current atherosclerosis reports* **17**, 485, doi:10.1007/s11883-014-0485-2 (2015).

26 Sukumaran, P. *et al.* Calcium Signaling Regulates Autophagy and Apoptosis. *Cells* **10**, doi:10.3390/cells10082125 (2021).

27 Scorrano, L. *et al.* BAX and BAK regulation of endoplasmic reticulum Ca2+: a control point for apoptosis. *Science (New York, N.Y.)* **300**, 135-139, doi:10.1126/science.1081208 (2003).

28 Son, D. J., Jung, J. C. & Hong, J. T. Epothilones Suppress Neointimal Thickening in the Rat Carotid Balloon-Injury Model by Inducing Vascular Smooth Muscle Cell Apoptosis through p53-Dependent Signaling Pathway. *PLoS One* **11**, e0155859, doi:10.1371/journal.pone.0155859 (2016).

29 Schlosser, A. *et al.* MFAP4 Promotes Vascular Smooth Muscle Migration, Proliferation and Accelerates Neointima Formation. *Arteriosclerosis, thrombosis, and vascular biology* **36**, 122-133, doi:10.1161/atvbaha.115.306672 (2016).

30 Chi, J. *et al.* Primary Culture of Rat Aortic Vascular Smooth Muscle Cells: A New Method. *Medical science monitor : international medical journal of experimental and clinical research* **23**, 4014-4020, doi:10.12659/msm.902816 (2017).

31 Ray, J. L., Leach, R., Herbert, J. M. & Benson, M. Isolation of vascular smooth muscle cells from a single murine aorta. *Methods in cell science : an official journal of the Society for In Vitro Biology* **23**, 185-188, doi:10.1023/a:1016357510143 (2001).

32 Kumar, P., Nagarajan, A. & Uchil, P. D. Analysis of Cell Viability by the MTT Assay. *Cold Spring Harbor protocols* **2018**, doi:10.1101/pdb.prot095505 (2018).

33 Gui, Y. & Zheng, X. L. Epidermal growth factor induction of phenotype-dependent cell cycle arrest in vascular smooth muscle cells is through the mitogen-activated protein kinase pathway. *The Journal of biological chemistry* **278**, 53017-53025, doi:10.1074/jbc.M309640200 (2003).

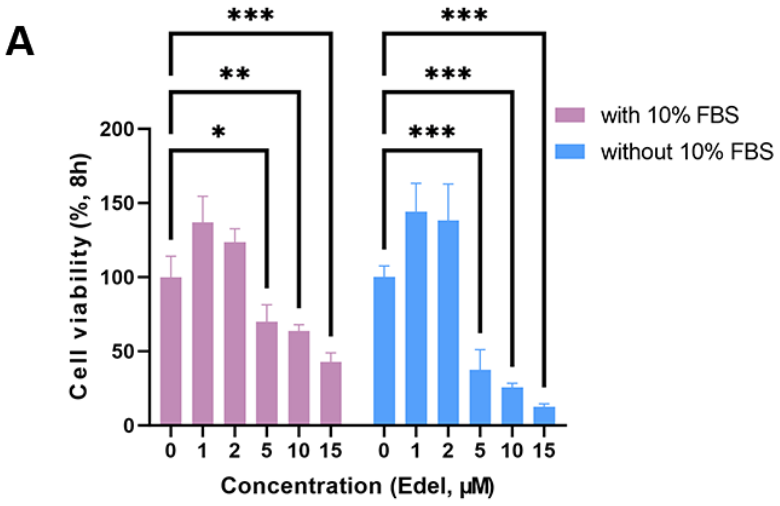

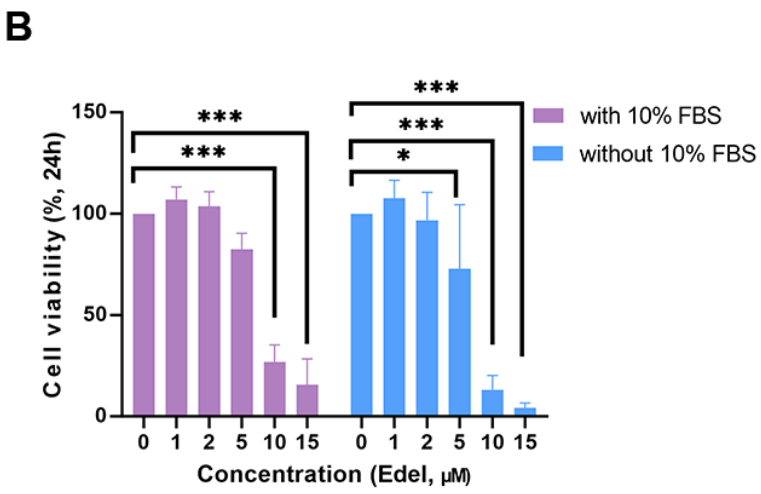

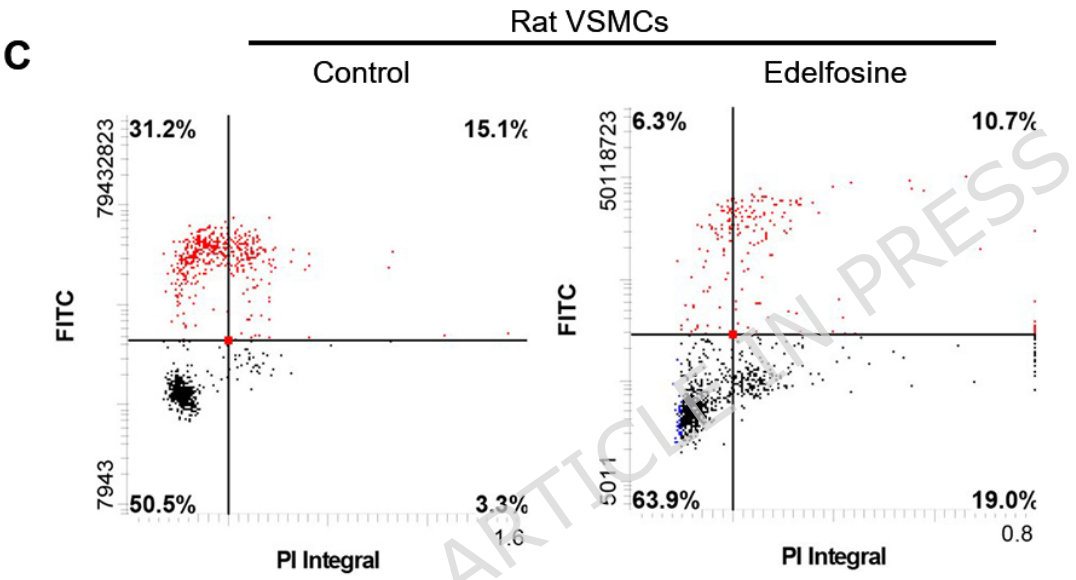

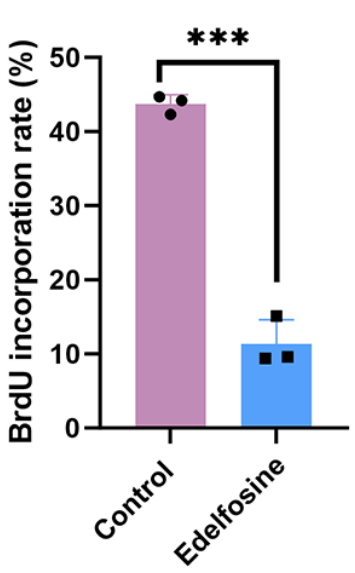

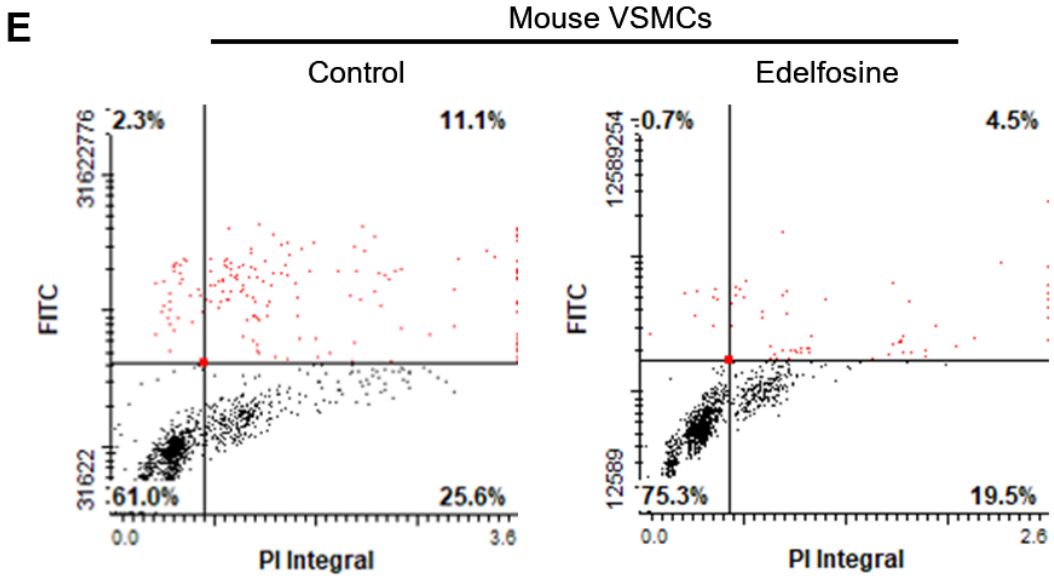

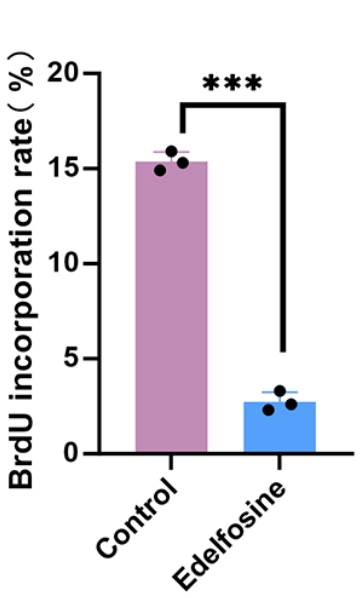

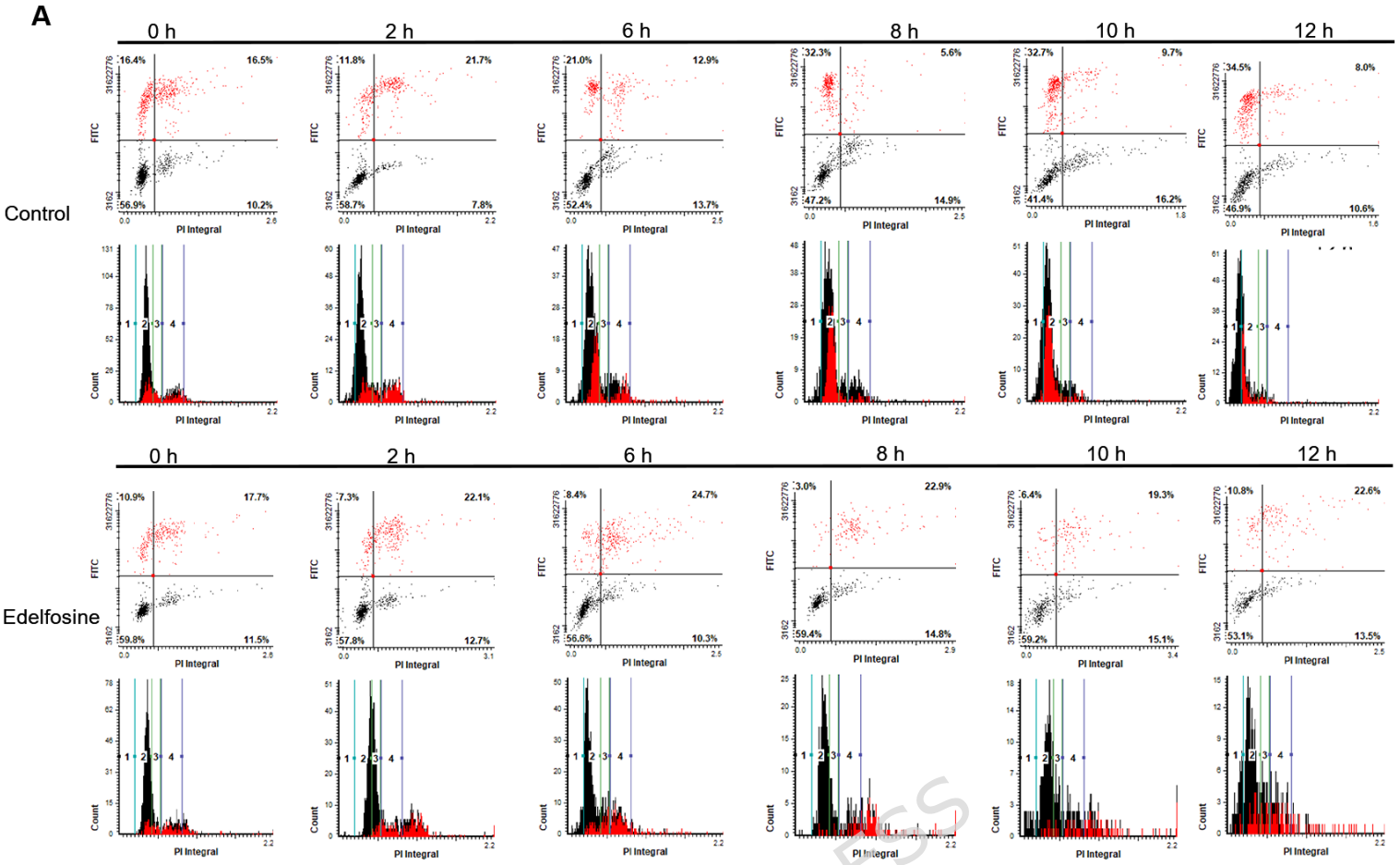

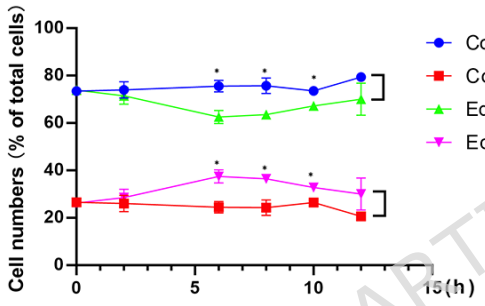

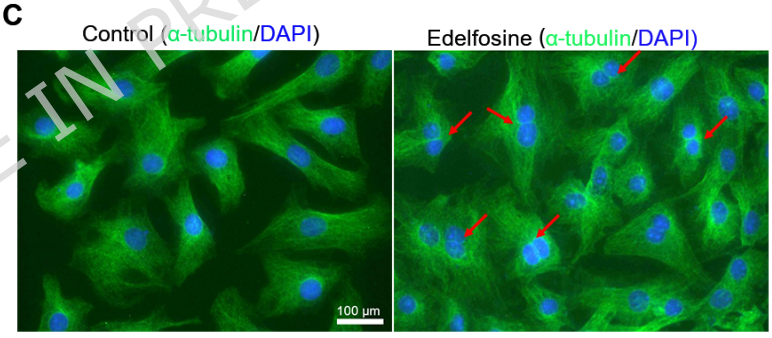

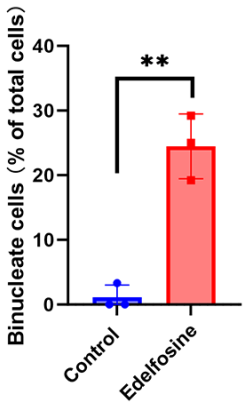

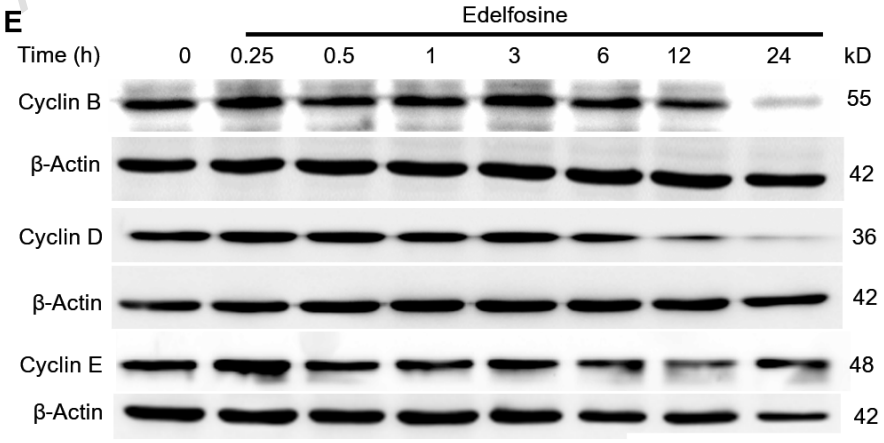

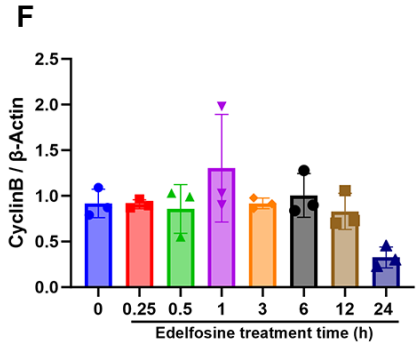

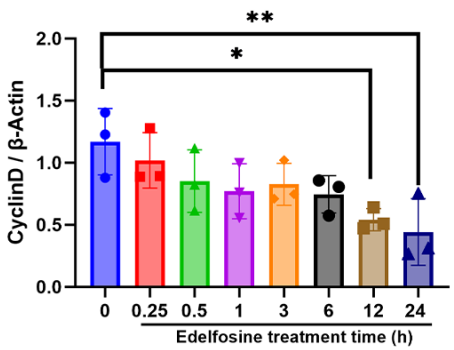

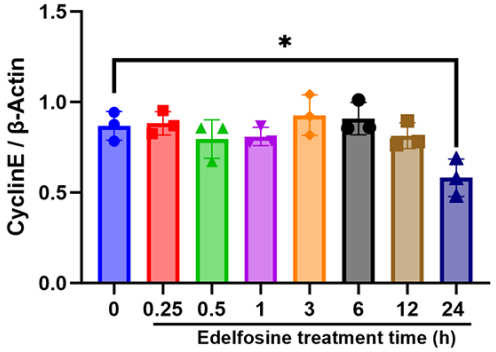

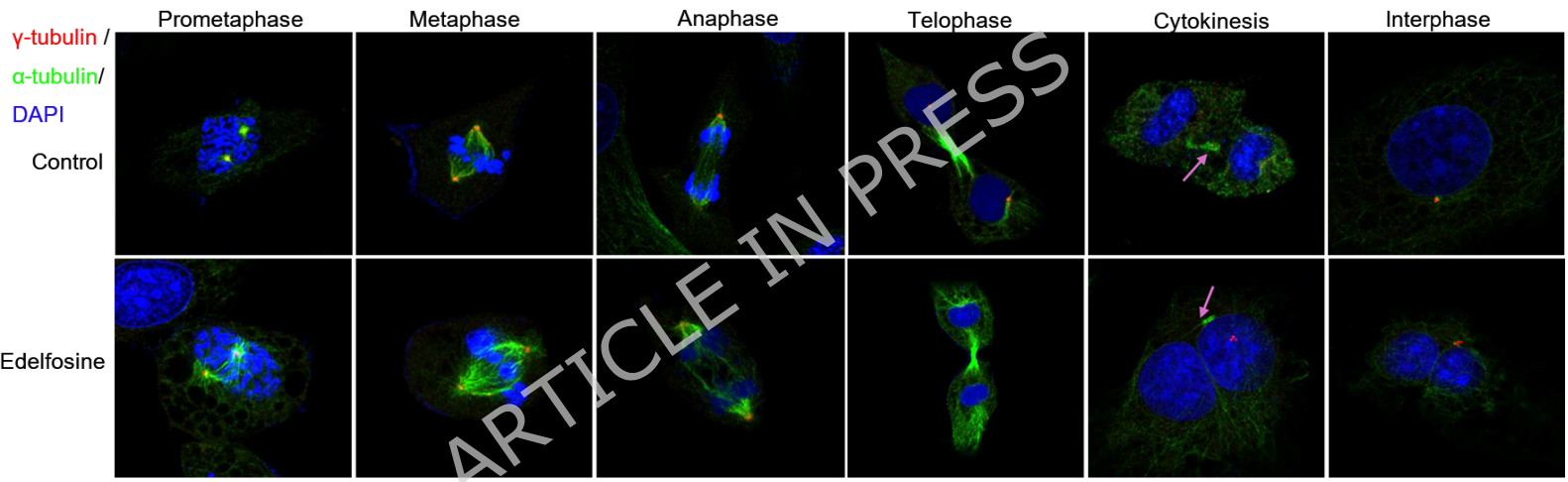

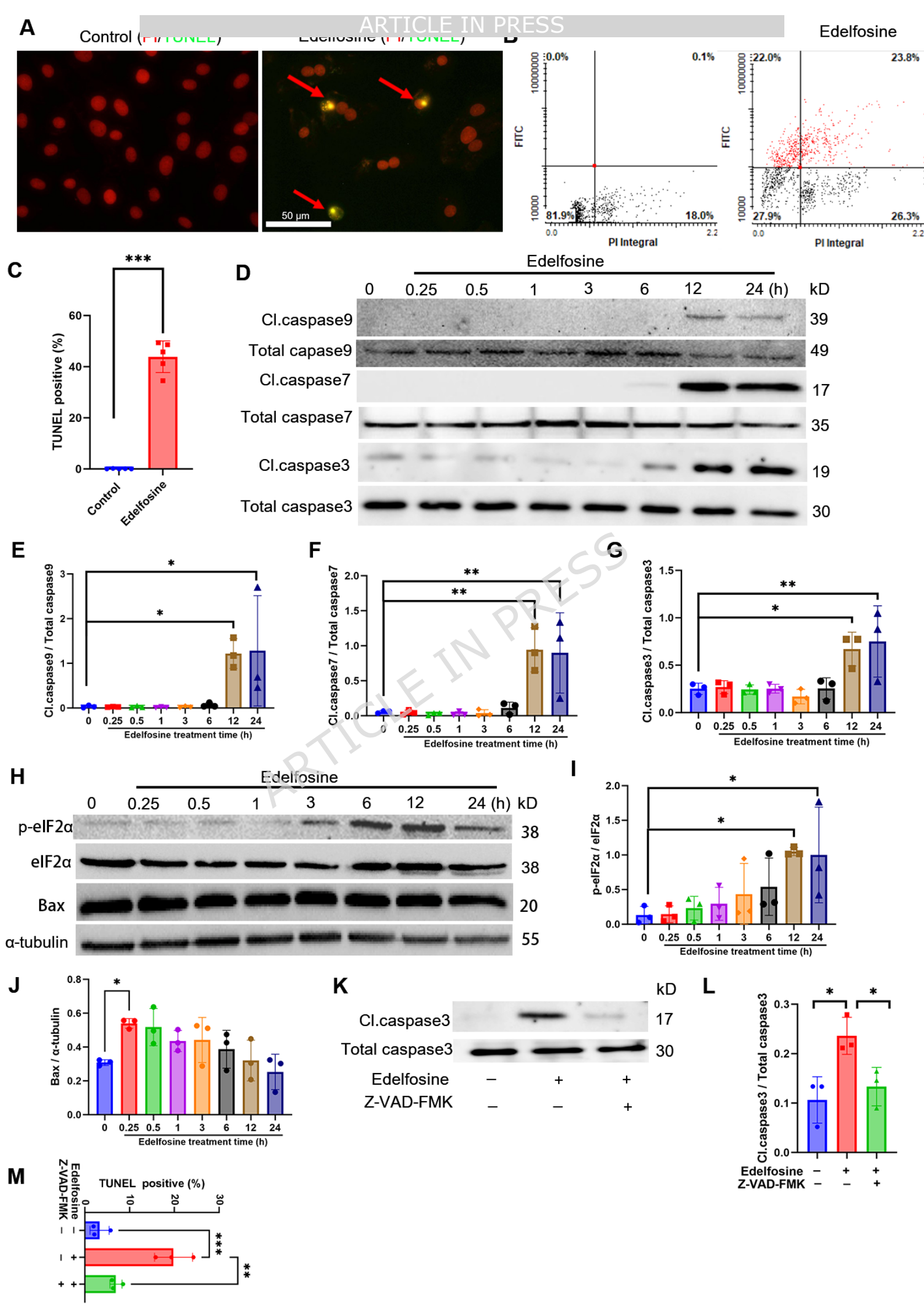

A

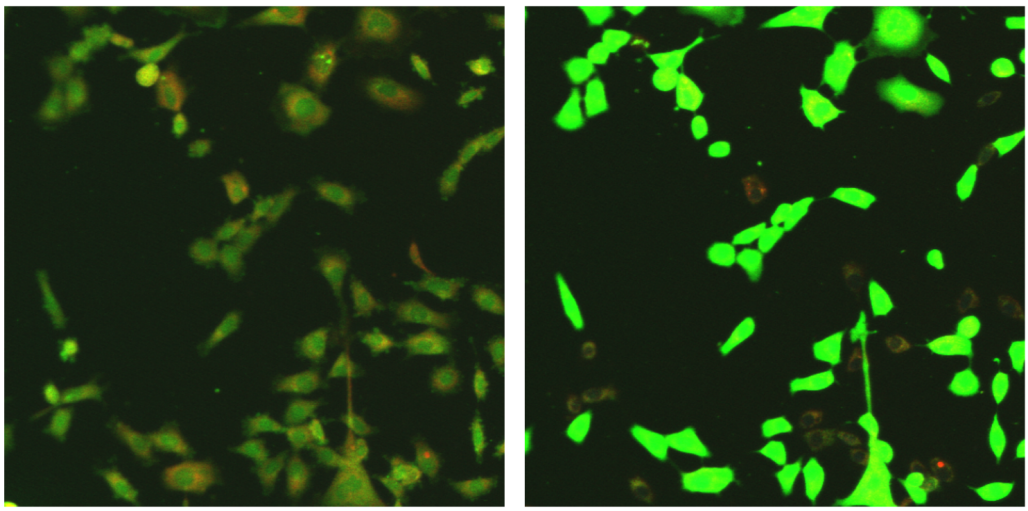

B

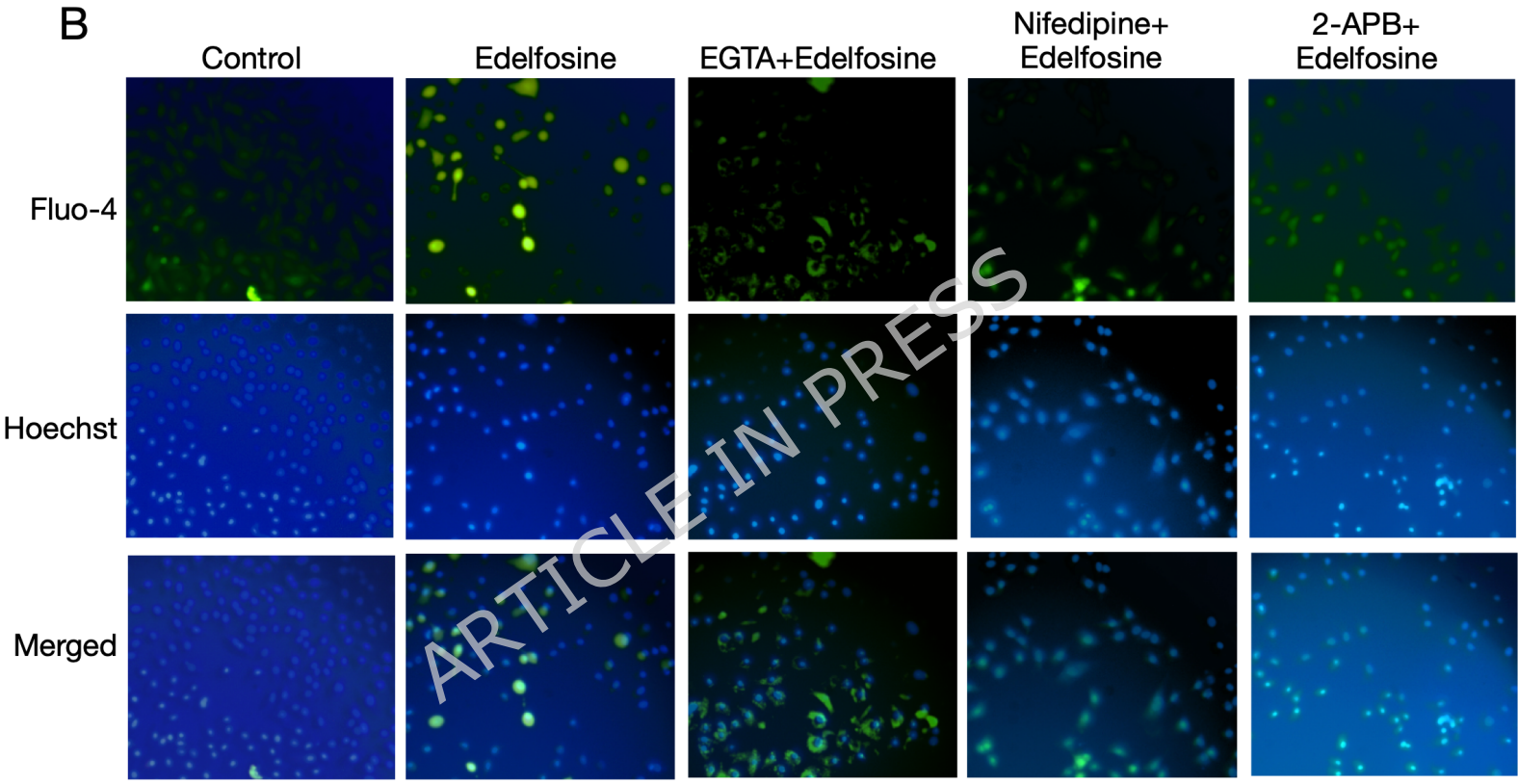

C